

Learning Robust Intervention Representations with Delta Embeddings

Panagiotis Alimisis, Christos Diou

Department of Informatics and Telematics, Harokopio University of Athens, Greece
 {csi23301, cdiou}@hua.gr

Abstract

Causal representation learning has attracted significant research interest during the past few years, as a means for improving model generalization and robustness. Causal representations of interventional image pairs, have the property that only variables corresponding to scene elements affected by the intervention / action are changed between the start state and the end state. While most work in this area has focused on identifying and representing the variables of the scene under a causal model, fewer efforts have focused on representations of the interventions themselves. In this work, we show that an effective strategy for improving out of distribution (OOD) robustness is to focus on the representation of interventions in the latent space. Specifically, we propose that an intervention can be represented by a Causal Delta Embedding that is invariant to the visual scene and sparse in terms of the causal variables it affects. Leveraging this insight, we propose a framework that is capable of learning causal representations from image pairs, without any additional supervision. Experiments in the Causal Triplet challenge demonstrate that Causal Delta Embeddings are highly effective in OOD settings, significantly exceeding baseline performance in both synthetic and real-world benchmarks.

Introduction

Understanding and reasoning about how the world changes in response to actions and external interventions is fundamental for artificial intelligence (AI) agents, especially those operating in dynamic environments. While deep learning models excel at learning complex patterns from data, they often struggle to generalize to new situations where the underlying data distribution changes, which is a critical limitation for real world deployment (Hendrycks et al. 2021; Geirhos et al. 2020). Recovering the true mechanisms that govern how data is generated and transformed is important for intelligent agents that can reason causally, as opposed to those that rely on statistical correlations (Pearl 2009).

This fundamental problem falls under the category of Causal Representation Learning (CRL) (Schölkopf et al. 2021), which focuses on disentangling the underlying causal variables of a system (Khemakhem et al. 2020). However, despite its importance in practical applications such as robotics or healthcare (Gupta et al. 2024; Hellström 2021; Sanchez et al. 2022), the specific challenge of learning robust, generalizable representations of the causal variables, as

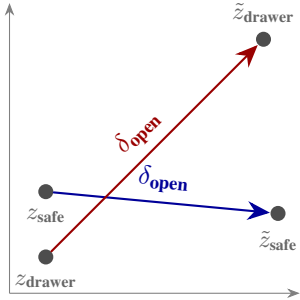
well as the interventions themselves remains an open problem.

A core challenge in building such robust causal AI systems lies in faithfully capturing the underlying data generation process. This is guided by two fundamental principles within CRL. First, the Independent Causal Mechanisms (ICM) posits that the distribution’s generative process can be decomposed into autonomous and independent modules, each representing a distinct causal mechanism (Peters, Janzing, and Schölkopf 2017; Schölkopf et al. 2021). Second, the Sparse Mechanism Shift (SMS) assumption suggests that an intervention typically affects only a small, localized subset of these causal mechanisms (Schölkopf et al. 2021). Most existing methods focus on identifying these disentangled factors from observations (Higgins et al. 2017; Khemakhem et al. 2020; Ahuja, Hartford, and Bengio 2022). Fewer methods, however, have focused on learning generalizable representations of the interventions, which can be equally important in predicting the outcome of interventions, especially when faced with novel situations.

In this paper, we introduce Causal Delta Embedding (CDE), a novel framework for learning robust representations of interventions from image pairs. Our core insight is that the intervention can be effectively isolated and represented as a delta embedding, the vector difference between the latent representations of pre- and post- intervention states if it satisfies the properties of (a) independence to causally irrelevant elements of the scene, in accordance to the ICM assumption (b) sparsity, in accordance to the SMS assumption and (c) object invariance, i.e., that the representation remains the same across objects. Using these properties as a guide, a learning strategy is proposed for learning CDEs from interventional image pairs.

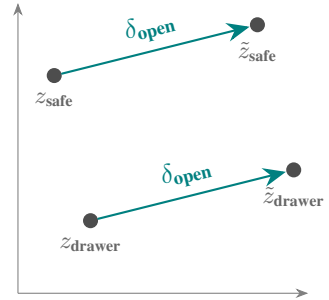
We evaluate CDE on the Causal Triplet challenge (Liu et al. 2023), which encompasses 3 increasingly complex settings: single-object synthetic data, multi-object synthetic data and real world scenes from EpicKitchens (Damen et al. 2022). Our experiments demonstrate that CDE establishes a new state of the art in OOD generalization for this challenge. Beyond quantitative performance, our analysis reveals that CDE learns a semantically structured intervention space, autonomously discovering anti-parallel relationships between opposing actions (e.g., open vs. close) without any explicit supervision.

Entangled Representations



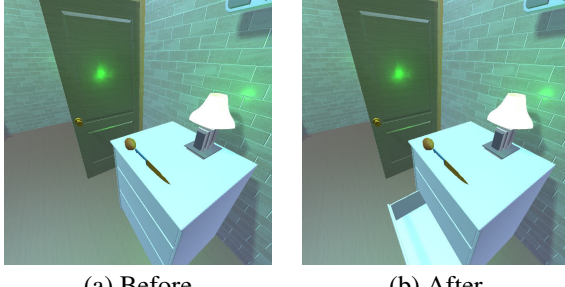
(a) Baseline Model (ERM). Action representations depend on the object and scene features.

Consistent Representations



(b) Causal Delta Embeddings. The action representation δ_{open} is invariant to the object and scene context.

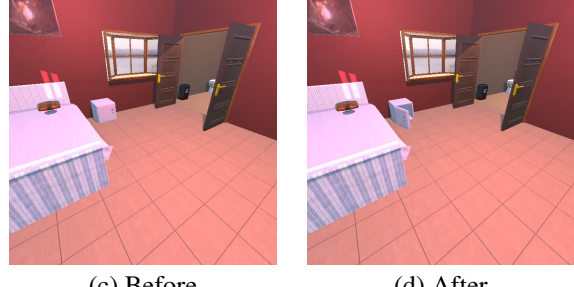
Drawer: Open



(a) Before

(b) After

Safe: Open



(c) Before

(d) After

(c) Examples of intervention pairs from our dataset, showing pre- and post-intervention states for various actions and objects.

Figure 1: Visualizing Causal Delta Embeddings. Unlike a baseline model that produces entangled representations of action vectors (left), our model learns object invariant action representations (right), that generalize well to out of distribution samples. The model is trained on intervention pairs like those shown at the bottom.

Our main contributions are as follows:

- We introduce *Causal Delta Embedding (CDE)*, a novel theoretical framework that explicitly defines the desiderata and learning principles for robustly representing interventions in a disentangled latent space.
- We propose a multi-objective loss function, designed to learn well separated, sparse and object invariant causal representations directly from visual data.
- We perform an extensive quantitative evaluation showing that our approach achieves state-of-the-art results in the Causal Triplet challenge.
- We show that our model discovers the semantic structure of the intervention space, including fundamental anti-parallel relationships between opposing actions, without any explicit supervision.

Related Work

Causal Representation Learning Part of the research on CRL focuses on identifying latent causal variables from high dimensional observations (Khemakhem et al. 2020; Ahuja, Hartford, and Bengio 2022). These methods established identifiability conditions for nonlinear ICA and demonstrated causal factor recovery under specific assumptions (Wendong et al. 2023; Monti, Zhang, and Hyvärinen 2020). Another

line of work focuses on causal disentanglement (Yang et al. 2021; Shen et al. 2020; Brehmer et al. 2022; Locatello et al. 2020a). These approaches often extend the Variational Autoencoder (VAE) framework (Kingma, Welling et al. 2013; Higgins et al. 2017). Object-centric learning methods have also been proposed in order to disentangle the visual scene into manipulable objects (Locatello et al. 2020b; Seitzer et al. 2022). More recent work has leveraged interventional data to improve causal disentanglement (Brehmer et al. 2022; Lippe et al. 2022; Squires et al. 2023; Lippe et al. 2023; Ahuja, Hartford, and Bengio 2022), showing that interventions provided crucial inductive biases for learning causal representations (Ahuja et al. 2023). While previous methods focus on identifying causal variables, our work instead models the interventional mechanisms, by learning generalizable embeddings that represent interventions in a way that remains invariant across different contexts.

Visual Action Recognition and OOD Generalization

Traditional action recognition methods rely on spatiotemporal patterns and achieve strong performance under IID conditions (Carreira and Zisserman 2017; Feichtenhofer et al. 2019; Arnab et al. 2021). However, these correlation-based approaches struggle with distribution shifts (Geirhos et al. 2020) and often are associated with spurious correlations (Wang and Jordan 2024). Recent work has explored

domain adaptation (Chen et al. 2019; Munro and Damen 2020) and causal approaches (Magliacane et al. 2018; Wang et al. 2023) for robust action understanding. Another category of methods uses large Vision Language Action (VLA) models (Kim et al. 2024; Zitkovich et al. 2023; Ma et al. 2024) to enable agents to perform actions in challenging environments. These models typically depend on large-scale pre-training on diverse data, yet generalization to unseen tasks remains an open challenge (Sapkota et al. 2025). Unlike these approaches, our method learns *causal* representations of interventions, in the sense that they satisfy properties resulting from the CRL assumptions. These representations are shown to generalize to novel object-action combinations without the need for finetuning.

Contrastive Learning and Sparse Representations
Contrastive learning has proven effective for learning meaningful representations by contrasting similar and dissimilar examples (Chen et al. 2020; Khosla et al. 2020). However, existing methods contrast individual samples, rather than relationships between samples. The principle of sparse mechanism shifts (Schölkopf et al. 2021; Peters, Janzing, and Schölkopf 2017), suggests that interventions affect only a small subset of the causal mechanisms. Sparsity in causal representations has been explored in various works (Pfister and Peters 2022; Xu et al. 2024) and has shown to improve disentanglement. However, combining sparsity with adversarial training (Liu et al. 2023) often leads to poor OOD performance, since other confounders might still be present in the scene, motivating our approach for stricter assumptions.

Problem Formulation

The central challenge this paper addresses is the development of a CRL framework that can robustly infer actions / interventions from high-dimensional observations, particularly under distribution shifts.

We formalize this challenge within the framework of the Structural Causal Model presented in (Liu et al. 2023) (Figure 2). Let us consider a set of causal variables $Z \in \mathcal{Z} \subset \mathbb{R}^l$, representing the state of the underlying data generating mechanisms. These variables have dependencies that are defined through a set of structural equations:

$$Z_i := f_i(\text{pa}(Z_i), \epsilon_i), \quad i = 1, \dots, l$$

where $\text{pa}(Z_i)$ denotes the set of causal parents of variable Z_i , and the ϵ_i are mutually independent stochastic noise terms representing unmodeled factors. The high-dimensional visual observation $x \in \mathcal{X} \subset \mathbb{R}^d$ is rendered from these latent variables via a complex, non-invertible generative function $g : \mathcal{Z} \rightarrow \mathcal{X}$, such that $x = g(Z)$.

We assume the latent space Z can be partitioned into scene-level variables Z_s (e.g., illumination, camera pose) and a set of object-level variables $Z_o = \{Z_{n,k}\}_{n=1, k=1}^{N, K}$, corresponding to the k -th property of the n -th object. An agent performs an action $a \in \mathcal{A}$, which performs an intervention on the system. This intervention transforms the pre-intervention state Z into a post-intervention state \tilde{Z} .

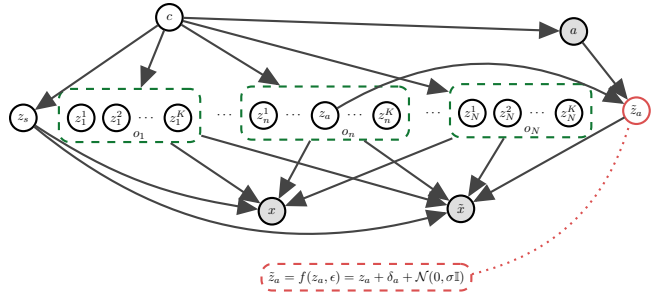


Figure 2: Causal Graph for a pair of observations (x, \tilde{x}) before and after an action a , proposed in (Liu et al. 2023). The data generating process is described by a set of latent factors, including global scene level factors z_s and local object level factors z_n^k , which are dependent due to confounders c . The action is assumed to influence only a few object level causal factors z_a in the scene and the effect of that influence is captured by \tilde{z}_a . The red dashed line indicates the structural equation assumed by our CDE approach.

Unobserved confounders (c) create spurious correlations and a training-testing distribution mismatch $P_{\text{train}}(Z, a) \neq P_{\text{test}}(Z, a)$. Following the *Independent Causal Mechanisms* principle (Schölkopf et al. 2012; Peters, Janzing, and Schölkopf 2017), we assume the true causal mechanism $P(\tilde{Z}_a | Z_a, a)$ is invariant to this shift. Therefore, a robust model must learn this invariant mechanism instead of non-stationary correlations.

We investigate two challenging types of OOD shifts:

- **Compositional Shifts:** Training and test sets share the same object classes, $O_{\text{train}} = O_{\text{test}}$, but disjoint sets of object-action pairs. $(A_{\text{train}} \times O_{\text{train}}) \cap (A_{\text{test}} \times O_{\text{test}}) = \emptyset$.
- **Systematic Shifts:** The training and test sets of object classes are disjoint, $O_{\text{train}} \cap O_{\text{test}} = \emptyset$.

Objective Given a dataset of paired observations $\mathcal{D} = \{(x, \tilde{x}, a)_j\}_{j=1}^M$, where x and \tilde{x} are the pre- and post-intervention images respectively, and a is the corresponding action label, our objective is to learn a function $\mathcal{F} : \mathcal{X} \times \mathcal{X} \rightarrow \mathcal{A}$. This function must predict the action a by learning a representation that isolates the invariant causal signature of the intervention, thereby achieving high performance on OOD test data characterized by the compositional and systematic shifts defined above.

Causal Delta Embeddings

Consider an *Encoder*, $\phi : \mathcal{X} \rightarrow \mathcal{Z}$ that maps a high-dimensional observation $x \in \mathcal{X}$ to a point in the latent space \mathcal{Z} . A Delta Embedding is defined as follows.

Definition 1 (Delta Embedding) Given a pair of observations (x, \tilde{x}) corresponding to the state of the world before and after an intervention $a \in \mathcal{A}$, the Delta Embedding, δ_a , is the vector difference

$$\delta_a := \phi(\tilde{x}) - \phi(x)$$

If the encoder is faithful to the data generating process illustrated by the model of Figure 2 and assuming identical noise across observations then for the Delta Embedding we have

$$\begin{aligned}\delta_a &= [z_s \ z_1 \ \cdots \ \tilde{z}_a \ \cdots z_N]^T - \\ &[z_s \ z_1 \ \cdots \ z_a \ \cdots z_N]^T \\ &= [0 \ \cdots \ \tilde{z}_a - z_a \ \cdots \ 0]^T\end{aligned}\quad (1)$$

where z_a is the dimension (or subset of dimensions) of object n that is affected by action a . From Eq. (1) we observe the following properties of δ_a .

1. **Independence.** Under the model of Figure 2, an action’s representation is independent of the causally irrelevant elements of the scene, i.e. scene properties and objects not affected by a .
2. **Sparsity.** If the assumption of *Sparse Mechanism Shifts* (Schölkopf et al. 2021; Liu et al. 2023) holds, then the action a will affect only a few underlying causal factors of the system, and the representation of the change, δ_a , will be sparse.

To generalize to novel compositions of actions and objects, the action representation must satisfy additional properties. Specifically, even if the *Independence* and *Sparsity* properties are satisfied, if the action a affects different objects in a different way, a learning system will not be able to predict how the action will modify the representations of unseen objects, or even seen objects but without any examples of these objects with a in the training set.

We therefore introduce an additional requirement on the action representation, namely that it remains similar when applied to different objects, e.g., that the representation of action *open* is fundamentally the same, regardless of whether it is a door or a box that is being opened. We therefore introduce an additional property:

3. **Invariance.** The action representation δ_a should not vary across different objects. One way to formalize this is through the variance of the delta embeddings across samples, i.e.,

$$\text{Var}_{x \sim P(X)}[\delta_a(x)] \approx 0 \quad (2)$$

Definition 2 (Causal Delta Embedding) A *Causal Delta Embedding (CDE)* is a Delta Embedding that satisfies the properties of *Independence*, *Sparsity* and *Invariance*.

In terms of the SCM of Figure 2, Causal Delta Embeddings can be implemented by defining the structural equation of \tilde{z}_a as

$$\tilde{z}_a = f(z_a, \epsilon) = z_a + \delta_a + \mathcal{N}(0, \sigma \mathbb{I}) \quad (3)$$

where σ is small. The following section uses this definition to develop a strategy for learning Causal Delta Embeddings.

Approach

The Global Causal Delta Embedding Model

We first introduce a *global* model, i.e., a model that learns a single causal representation from the entire image.

Model Architecture The model consists of three main components, as illustrated in Figure 3 (A).

1. **The Encoder (ϕ):** The encoder is responsible for mapping an input image x into the \mathcal{Z} . It is composed of two sub-modules:

- **A Pre-trained Vision Backbone:** We use a powerful Vision Transformer (ViT) (Dosovitskiy et al. 2020), specifically one pre-trained with the DINO self-supervision algorithm (Caron et al. 2021). The backbone processes the input image and outputs a high-dimensional feature vector. We use the output corresponding to the ‘[CLS]’ token as the global image representation.

- **A Causal Projector:** The feature vector from the backbone is then passed through a small multi-layer perceptron (MLP). This projector’s role is to transform the general-purpose features into an l -dimensional representation satisfying the Causal Delta Embedding properties.

2. **Delta Computation:** Following Definition 1, the core of our method is the computation of the Causal Delta Embedding. Given the latent vectors for the pre-intervention image ($z = \phi(x)$) and post-intervention image ($\tilde{z} = \phi(\tilde{x})$), the delta is calculated via simple, element-wise subtraction:

$$\delta = \tilde{z} - z$$

3. **The Action Classifier (h):** The resulting delta vector δ is the sole input to a final classification head. This head is another small MLP that takes the l -dimensional delta and outputs logits for the different action classes in \mathcal{A} .

Implementation of the Learning Objective To train the model and learn the Causal Delta Embeddings satisfying the properties outlined in the previous section, we combine three loss functions.

1. **Cross-Entropy Loss:** The primary objective is to ensure the delta embedding is useful for the downstream task. We use a standard Cross-Entropy loss, \mathcal{L}_{CE} between the predicted action logits $h(\delta_i)$ and the one-hot ground-truth action label a_i .
2. **Supervised Contrastive Loss:** To enforce that embeddings for the same action are clustered together (Property 3, Invariance), we employ the Supervised Contrastive Loss, $\mathcal{L}_{\text{contrast}}$ (Khosla et al. 2020). For a batch of B delta embeddings, the loss for each embedding δ_i (the “anchor”) encourages it to be closer to other embeddings of the same class (“positives”) than to all other embeddings in the batch.

$$\mathcal{L}_{\text{contrast}} = \sum_{i=1}^B \frac{-1}{|P(i)|} \sum_{p \in P(i)} \log \frac{\exp(\text{sim}(\delta_i, \delta_p)/\tau)}{\sum_{j \neq i} \exp(\text{sim}(\delta_i, \delta_j)/\tau)} \quad (4)$$

where $P(i)$ is the set of all positive samples for anchor i in the batch, $\text{sim}(\cdot, \cdot)$ denotes the cosine similarity, and τ is a scalar temperature hyperparameter. This loss component is also consistent with the structural equation (3).

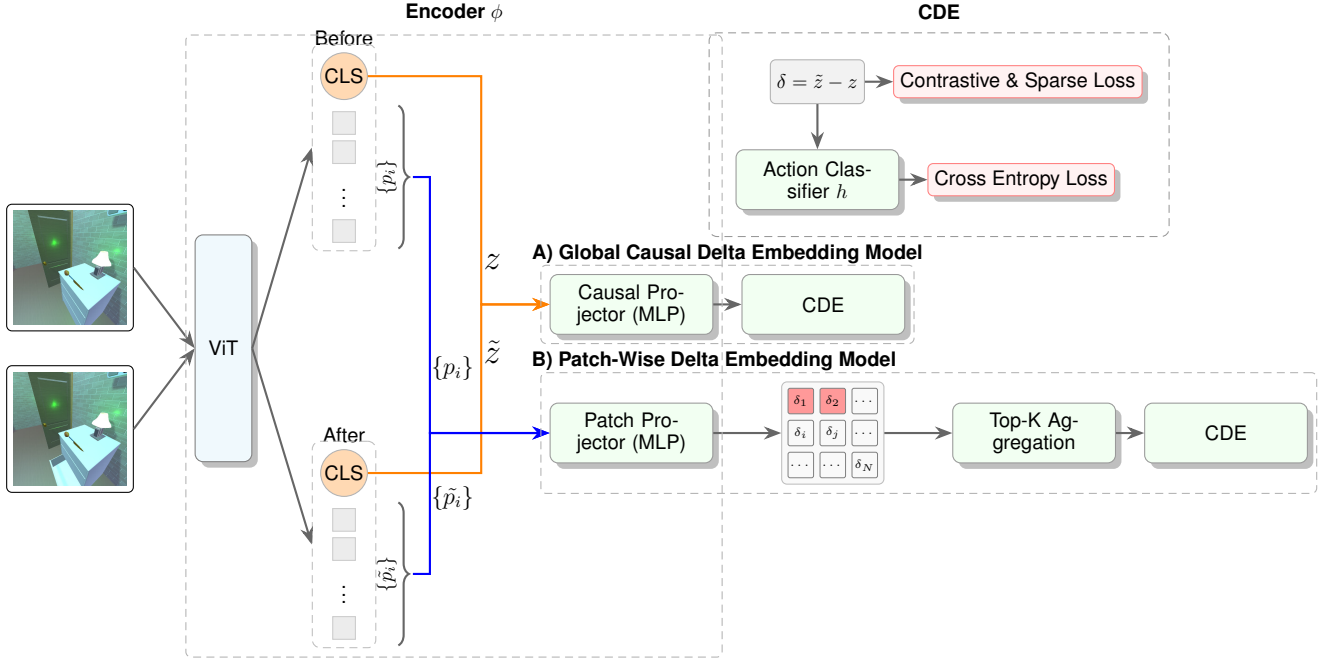


Figure 3: Model architecture. Model A (top) computes a global causal delta from CLS tokens. Model B (bottom) computes patch-wise deltas, aggregated to a causal delta. Both feed into a common action classifier.

3. **Sparsity Regularizer:** To encourage a minimal representation in line with the sparse mechanism shift hypothesis (Property 2, Sparsity), we apply an ℓ_1 regularization penalty. This loss penalizes the sum of the absolute values of the embedding dimensions, promoting solutions where most dimensions are zero.

$$\mathcal{L}_{\text{sparsity}} = \frac{1}{B} \sum_{i=1}^B \|\delta_i\|_1 = \frac{1}{B} \sum_{i=1}^B \sum_{k=1}^l |\delta_{i,k}| \quad (5)$$

The final training objective is a weighted sum of these three components:

$$\mathcal{L}_{\text{total}} = \mathcal{L}_{\text{CE}} + \alpha_{\text{contrast}} \mathcal{L}_{\text{contrast}} + \alpha_{\text{sparsity}} \mathcal{L}_{\text{sparsity}} \quad (6)$$

where α_{contrast} and α_{sparsity} are scalar hyperparameters that balance the influence of each loss component.

Notice that although no loss component explicitly enforces Property 1, this property is directly satisfied by the use of the Delta Embedding and image pairs, where the observed changes are only due to a . This does not hold under the actionable counterfactual case (Liu et al. 2023), where additional scene variables may change across observations. If, however, these changes are not spuriously correlated with the action a in the data, then the use of \mathcal{L}_{CE} can still retrieve the CDE representation. A deeper investigation of the actionable counterfactual case is left as future work.

Spatial Extension: The Patch-Wise Model

Motivation In complex scenes with multiple objects or significant background noise, an action may only affect a small, localized region of the image. A global embedding

risks ‘averaging out’ this important local change, making it difficult to detect. To address this, we developed a patch-wise extension of our model.

Architecture The Patch-Wise model adapts the core architecture to operate on local regions, as shown in Figure 3 (B).

1. **Patch-wise Feature Extraction:** We use a ViT backbone, but instead of taking the global ‘[CLS]’ token, we retain the output feature vectors for each individual image patch. This gives us a sequence of patch features for both the before and after images.
2. **Patch-wise Delta Computation:** A shared Causal Projector and the subtraction operation are applied independently to each corresponding pair of patch features. This yields a set of delta embeddings, $\{\delta_p\}$, one for each spatial patch location p .
3. **The Aggregation Module (\mathcal{G}):** Since the action classifier needs a single input vector, we must aggregate the set of patch-wise deltas. This module’s task is to identify the region of change and produce a single, representative delta vector $\bar{\delta}$. We employed the following simple and effective aggregation strategy:
Top-K Aggregation: This strategy is based on the assumption that the action’s primary effect is localized to a few patches. We identify the k patches with the largest change by measuring the L_2 norm of their delta vectors ($\|\delta_p\|_2$). The final delta $\bar{\delta}$ is the average of these top k patch deltas.

The same loss function ($\mathcal{L}_{\text{total}}$) is then applied to the aggregated delta vector $\bar{\delta}$.

Table 1: Single-object ProcTHOR results. Our Global Delta Embedding model significantly improves OOD generalization under both compositional and systematic shifts. (R: ResNet-18, V: Vit-Small)

Method	IID Acc.	OOD Comp.	OOD Syst.	Gap Syst. (\downarrow)
Vanilla-R	0.96 ± 0.01	0.36 ± 0.13	0.48 ± 0.08	0.48
Vanilla-V	0.95 ± 0.01	0.34 ± 0.27	0.47 ± 0.11	0.48
ICM-R	0.95 ± 0.01	0.41 ± 0.15	0.50 ± 0.09	0.45
ICM-V	0.95 ± 0.01	0.38 ± 0.26	0.49 ± 0.01	0.46
SMS-R	0.96 ± 0.01	0.47 ± 0.18	0.54 ± 0.07	0.42
SMS-V	0.95 ± 0.01	0.34 ± 0.27	0.39 ± 0.04	0.56
Ours_(Global)	0.96 ± 0.01	0.91 ± 0.02	0.73 ± 0.02	0.18

Experiments

This section evaluates the effectiveness of our CDE framework. We first describe our experimental setup, then present the main quantitative results demonstrating CDE’s effectiveness in OOD generalization, followed by qualitative and ablation analyses that provide deeper insights into its learned representations and design choices.

Experimental Setup

Our evaluation is conducted on the Causal Triplet benchmark (Liu et al. 2023), specifically designed for intervention-centric causal representation learning. This benchmark features three distinct settings of increasing visual complexity: single-object synthetic scenes, multi-object synthetic scenes (both from ProcTHOR (Deitke et al. 2022)), and challenging real-world scenes from Epic-Kitchens (Damen et al. 2022). In all settings models are trained on pairs of pre- and post-intervention images with action labels and are evaluated for their ability to infer the action. Further details on the datasets and data filtering procedures are provided in the Appendix.

We follow the Causal Triplet protocol, evaluating models on both IID and OOD test sets. The OOD splits test two forms of generalization: *Compositional Distribution Shifts*, where the model encounters unseen combinations of actions and objects (e.g., `open(drawer)` when only `open(door)` and `close(drawer)` were seen during training); and *Systematic Distribution Shifts*, where generalization to entirely unseen object classes is required. Visualizations of these distribution shifts are available in the Appendix. All reported quantitative results are mean accuracies and standard deviations average over 3 random seeds. We set $\alpha_{\text{contrast}} = 2.0$ and $\alpha_{\text{sparsity}} = 1.0$ for all experiments (see the Appendix for more details).

We compare our two proposed models against the baselines from the Causal Triplet paper (Liu et al. 2023), including vanilla ResNets (He et al. 2016), methods incorporating causal regularization (ICM, SMS), and object-centric approaches (Slot Attention (Locatello et al. 2020b), GroupViT (Xu et al. 2022)).

Table 2: Multi-object ProcTHOR results (systematic shift). Our Patch-Wise model outperforms all baselines, including oracle methods.

Method	IID Acc.	OOD Acc.	Gap (\downarrow)
ResNet	0.83 ± 0.01	0.30 ± 0.08	0.53
Oracle-mask	0.90 ± 0.01	0.42 ± 0.06	0.48
Slot-avg	0.49 ± 0.01	0.15 ± 0.01	0.34
Slot-dense	0.51 ± 0.01	0.19 ± 0.03	0.32
Slot-match	0.66 ± 0.01	0.21 ± 0.01	0.45
Ours_(Patch-wise)	0.92 ± 0.01	0.45 ± 0.02	0.47

Table 3: Real-world Epic-Kitchens results (systematic shift). Our method shows robust performance improvements in a challenging, unconstrained setting.

Method	IID Acc.	OOD Acc.	Gap (\downarrow)
ResNet	0.42 ± 0.03	0.17 ± 0.03	0.25
CLIP	0.45 ± 0.02	0.24 ± 0.02	0.21
Group-avg	0.47 ± 0.03	0.24 ± 0.03	0.23
Group-dense	0.50 ± 0.04	0.26 ± 0.03	0.24
Group-token	0.52 ± 0.03	0.27 ± 0.03	0.25
Ours_(Patch-wise)	0.55 ± 0.02	0.33 ± 0.02	0.22

Main Quantitative Results

Our CDE framework consistently delivers substantial improvements in OOD robustness across all evaluation settings, establishing a new state of the art. Our models show remarkable OOD generalization across all evaluation settings. For single-object scenes, our global CDE model cuts the generalization gap from 0.56 to 0.18 while matching IID accuracy (Table 1). In challenging multi-object and real-world settings (Tables 2 and 3), our Patch-Wise model outperforms all baselines, including oracle methods that use ground-truth segmentations masks. This validates our unsupervised approach, which boosts OOD accuracy by 6 points on the noisy Epic-Kitchens dataset.

In summary, across all three levels of complexity, our Causal Delta Embedding framework consistently delivers substantial improvements in OOD robustness, showcasing its ability to learn invariant representations of causal actions.

Further Analysis

While our model demonstrates state-of-the-art out-of-distribution (OOD) accuracy, a deeper analysis is required to verify that this performance stems from the successful implementation of the theoretical properties of Causal Delta Embeddings.

Action Relationships in Causal Delta Space

To study the semantic structure of the learned delta space, we investigated whether the model could discover fundamental relationships between actions on its own. We computed the pairwise cosine similarity between all learned ac-



Figure 4: Heatmap of pairwise cosine similarities between all learned delta embeddings. The strong blue squares (similarity near -1.0) reveal a near-perfect anti-parallel relationship for opposite action pairs, which was discovered entirely from the data.

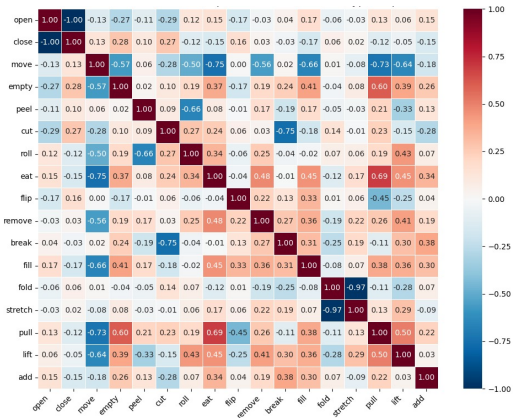


Figure 5: Heatmap of pairwise cosine similarities between all learned action prototypes for the EpicKitchens dataset.

tion representations and visualized the result in a similarity matrix (Figure 4). The analysis reveals the following property: the model has learned a perfect *anti-parallel relationship* for opposite actions. The cosine similarity between the prototypes for `open` and `close`, for `dirty` and `clean`, and for `turn on` and `turn off`, is -1.0. This demonstrates that our framework not only separates the action concepts but also discovers opposing relationships between them, organizing the representations in a meaningful way. Furthermore we can see that a similar pattern occurs in the most challenging real-world dataset where the model learns the anti-parallel relationships for the actions `open` and `close` and also for `fold` and `stretch` (Figure 5).

In summary, the combination of strong predictive properties and consistent semantic structure demonstrates that our CDE framework learns meaningful representations of interventions. For further geometric analysis of the delta space, including UMAP projections and k-NN classifier performance, refer to the Appendix.

Table 4: Ablation study of our method’s components on the ViT-Small model. Results are for the single-object systematic shift setting, showing the impact on OOD accuracy when each core component is removed.

Model Configuration	IID Acc. (%)	OOD Acc. (%)
Full Model	0.95	0.73
<i>Ablations</i>		
w/o Sparsity Loss	0.96	0.70
w/o Contrastive Loss	0.95	0.60
Baseline (CE Loss only)	0.94	0.59

Ablation Study

To understand the contribution of each component of our CDE framework, we conducted a series of ablation studies. We analyze the impact of each major loss component on the performance of our primary model with a ViT-Small backbone. Table 4 presents the results, comparing our full model against versions where each theoretical component is removed, and a baseline trained only with standard CE loss.

The results demonstrate the effectiveness of our approach. Our full model achieves an OOD accuracy of 73.0%, a +14 point improvement over the baseline trained solely with a CE objective, validating that explicitly structuring the representation space is critical for generalization. The supervised contrastive loss causes a 13-point drop in OOD accuracy when removed. The sparsity loss term causes a 3-point drop when removed.

For more ablation studies, refer to the Appendix.

Conclusion

This paper introduces the *Causal Delta Embedding (CDE)* framework, a simple yet effective approach to interventional causal representation learning. By explicitly modeling interventions as delta vectors in a structured latent space, CDE inherently satisfies the properties of independence, sparsity and invariance, leading to improved generalization. Our empirical validation on the Causal Triplet challenge demonstrates that CDE achieves state-of-the-art OOD generalization, outperforming prior methods across synthetic and real world datasets. Beyond quantitative gains, we show that CDE learns semantically meaningful representations without supervision, where opposing actions have anti-parallel representations. Despite the promising results, we acknowledge that limitations remain for real-world data, since both IID and OOD accuracies are still low for real world deployment, and also the use of universal delta embeddings for each action limits its ability to capture context-dependent visual transformations of actions. Future research directions include dynamically identifying modified regions of the input states through attention mechanisms, extending the framework to video streams for modeling causal dynamics in temporal sequences, and investigating compositional properties of delta embeddings to enable multi-step interventions and generalization to novel action sequences.

References

Ahuja, K.; Hartford, J. S.; and Bengio, Y. 2022. Weakly supervised representation learning with sparse perturbations. *Advances in Neural Information Processing Systems*, 35: 15516–15528.

Ahuja, K.; Mahajan, D.; Wang, Y.; and Bengio, Y. 2023. Interventional causal representation learning. In *International conference on machine learning*, 372–407. PMLR.

Arnab, A.; Dehghani, M.; Heigold, G.; Sun, C.; Lučić, M.; and Schmid, C. 2021. Vivit: A video vision transformer. In *Proceedings of the IEEE/CVF international conference on computer vision*, 6836–6846.

Brehmer, J.; De Haan, P.; Lippe, P.; and Cohen, T. S. 2022. Weakly supervised causal representation learning. *Advances in Neural Information Processing Systems*, 35: 38319–38331.

Caron, M.; Touvron, H.; Misra, I.; Jégou, H.; Mairal, J.; Bojanowski, P.; and Joulin, A. 2021. Emerging properties in self-supervised vision transformers. In *Proceedings of the IEEE/CVF international conference on computer vision*, 9650–9660.

Carreira, J.; and Zisserman, A. 2017. Quo vadis, action recognition? a new model and the kinetics dataset. In *proceedings of the IEEE Conference on Computer Vision and Pattern Recognition*, 6299–6308.

Chen, M.-H.; Kira, Z.; AlRegib, G.; Yoo, J.; Chen, R.; and Zheng, J. 2019. Temporal attentive alignment for large-scale video domain adaptation. In *Proceedings of the IEEE/CVF international conference on computer vision*, 6321–6330.

Chen, T.; Kornblith, S.; Norouzi, M.; and Hinton, G. 2020. A simple framework for contrastive learning of visual representations. In *International conference on machine learning*, 1597–1607. PmLR.

Damen, D.; Doughty, H.; Farinella, G. M.; Furnari, A.; Kazakos, E.; Ma, J.; Moltisanti, D.; Munro, J.; Perrett, T.; Price, W.; et al. 2022. Rescaling egocentric vision: Collection, pipeline and challenges for epic-kitchens-100. *International Journal of Computer Vision*, 1–23.

Deitke, M.; VanderBilt, E.; Herrasti, A.; Weihs, L.; Ehsani, K.; Salvador, J.; Han, W.; Kolve, E.; Kembhavi, A.; and Mottaghi, R. 2022. ProcTHOR: Large-Scale Embodied AI Using Procedural Generation. *Advances in Neural Information Processing Systems*, 35: 5982–5994.

Dosovitskiy, A.; Beyer, L.; Kolesnikov, A.; Weissenborn, D.; Zhai, X.; Unterthiner, T.; Dehghani, M.; Minderer, M.; Heigold, G.; Gelly, S.; et al. 2020. An image is worth 16x16 words: Transformers for image recognition at scale. *arXiv preprint arXiv:2010.11929*.

Feichtenhofer, C.; Fan, H.; Malik, J.; and He, K. 2019. Slowfast networks for video recognition. In *Proceedings of the IEEE/CVF international conference on computer vision*, 6202–6211.

Geirhos, R.; Jacobsen, J.-H.; Michaelis, C.; Zemel, R.; Brendel, W.; Bethge, M.; and Wichmann, F. A. 2020. Shortcut learning in deep neural networks. *Nature Machine Intelligence*, 2(11): 665–673.

Gupta, T.; Gong, W.; Ma, C.; Pawlowski, N.; Hilmkil, A.; Scetbon, M.; Rigter, M.; Famoti, A.; Llorens, A. J.; Gao, J.; et al. 2024. The essential role of causality in foundation world models for embodied ai. *arXiv preprint arXiv:2402.06665*.

He, K.; Zhang, X.; Ren, S.; and Sun, J. 2016. Deep residual learning for image recognition. In *Proceedings of the IEEE conference on computer vision and pattern recognition*, 770–778.

Hellström, T. 2021. The relevance of causation in robotics: A review, categorization, and analysis. *Paladyn, Journal of Behavioral Robotics*, 12(1): 238–255.

Hendrycks, D.; Basart, S.; Mu, N.; Kadavath, S.; Wang, F.; Dorundo, E.; Desai, R.; Zhu, T.; Parajuli, S.; Guo, M.; et al. 2021. The many faces of robustness: A critical analysis of out-of-distribution generalization. In *Proceedings of the IEEE/CVF international conference on computer vision*, 8340–8349.

Higgins, I.; Matthey, L.; Pal, A.; Burgess, C.; Glorot, X.; Botvinick, M.; Mohamed, S.; and Lerchner, A. 2017. beta-vae: Learning basic visual concepts with a constrained variational framework. In *International conference on learning representations*.

Khemakhem, I.; Kingma, D.; Monti, R.; and Hyvarinen, A. 2020. Variational autoencoders and nonlinear ica: A unifying framework. In *International conference on artificial intelligence and statistics*, 2207–2217. PMLR.

Khosla, P.; Teterwak, P.; Wang, C.; Sarna, A.; Tian, Y.; Isola, P.; Maschinot, A.; Liu, C.; and Krishnan, D. 2020. Supervised contrastive learning. *Advances in neural information processing systems*, 33: 18661–18673.

Kim, M. J.; Pertsch, K.; Karamchetti, S.; Xiao, T.; Balakrishna, A.; Nair, S.; Rafailov, R.; Foster, E.; Lam, G.; Sanketi, P.; et al. 2024. Openvla: An open-source vision-language-action model. *arXiv preprint arXiv:2406.09246*.

Kingma, D. P.; Welling, M.; et al. 2013. Auto-encoding variational bayes.

Lippe, P.; Magliacane, S.; Löwe, S.; Asano, Y. M.; Cohen, T.; and Gavves, E. 2023. Biscuit: Causal representation learning from binary interactions. In *Uncertainty in Artificial Intelligence*, 1263–1273. PMLR.

Lippe, P.; Magliacane, S.; Löwe, S.; Asano, Y. M.; Cohen, T.; and Gavves, S. 2022. Citris: Causal identifiability from temporal intervened sequences. In *International Conference on Machine Learning*, 13557–13603. PMLR.

Liu, S.; Zeng, Z.; Ren, T.; Li, F.; Zhang, H.; Yang, J.; Jiang, Q.; Li, C.; Yang, J.; Su, H.; et al. 2024. Grounding dino: Marrying dino with grounded pre-training for open-set object detection. In *European Conference on Computer Vision*, 38–55. Springer.

Liu, Y.; Alahi, A.; Russell, C.; Horn, M.; Zietlow, D.; Schölkopf, B.; and Locatello, F. 2023. Causal triplet: An open challenge for intervention-centric causal representation learning. In *Conference on Causal Learning and Reasoning*, 553–573. PMLR.

Locatello, F.; Poole, B.; Rätsch, G.; Schölkopf, B.; Bachem, O.; and Tschannen, M. 2020a. Weakly-supervised disentanglement without compromises. In *International conference on machine learning*, 6348–6359. PMLR.

Locatello, F.; Weissenborn, D.; Unterthiner, T.; Mahendran, A.; Heigold, G.; Uszkoreit, J.; Dosovitskiy, A.; and Kipf, T. 2020b. Object-centric learning with slot attention. *Advances in neural information processing systems*, 33: 11525–11538.

Loshchilov, I.; and Hutter, F. 2017. Decoupled weight decay regularization. *arXiv preprint arXiv:1711.05101*.

Ma, Y.; Song, Z.; Zhuang, Y.; Hao, J.; and King, I. 2024. A survey on vision-language-action models for embodied ai. *arXiv preprint arXiv:2405.14093*.

Magliacane, S.; Van Ommen, T.; Claassen, T.; Bongers, S.; Versteeg, P.; and Mooij, J. M. 2018. Domain adaptation by using causal inference to predict invariant conditional distributions. *Advances in neural information processing systems*, 31.

Monti, R. P.; Zhang, K.; and Hyvärinen, A. 2020. Causal discovery with general non-linear relationships using non-linear ICA. In *Uncertainty in artificial intelligence*, 186–195. PMLR.

Munro, J.; and Damen, D. 2020. Multi-modal domain adaptation for fine-grained action recognition. In *Proceedings of the IEEE/CVF conference on computer vision and pattern recognition*, 122–132.

Pearl, J. 2009. *Causality*. Cambridge university press.

Peters, J.; Janzing, D.; and Schölkopf, B. 2017. *Elements of causal inference: foundations and learning algorithms*. The MIT Press.

Pfister, N.; and Peters, J. 2022. Identifiability of sparse causal effects using instrumental variables. In *Uncertainty in Artificial Intelligence*, 1613–1622. PMLR.

Sanchez, P.; Voisey, J. P.; Xia, T.; Watson, H. I.; O’Neil, A. Q.; and Tsaftaris, S. A. 2022. Causal machine learning for healthcare and precision medicine. *Royal Society Open Science*, 9(8): 220638.

Sapkota, R.; Cao, Y.; Roumeliotis, K. I.; and Karkee, M. 2025. Vision-language-action models: Concepts, progress, applications and challenges. *arXiv preprint arXiv:2505.04769*.

Schölkopf, B.; Janzing, D.; Peters, J.; Sgouritsa, E.; Zhang, K.; and Mooij, J. 2012. On causal and anticausal learning. *arXiv preprint arXiv:1206.6471*.

Schölkopf, B.; Locatello, F.; Bauer, S.; Ke, N. R.; Kalchbrenner, N.; Goyal, A.; and Bengio, Y. 2021. Toward causal representation learning. *Proceedings of the IEEE*, 109(5): 612–634.

Seitzer, M.; Horn, M.; Zadaianchuk, A.; Zietlow, D.; Xiao, T.; Simon-Gabriel, C.-J.; He, T.; Zhang, Z.; Schölkopf, B.; Brox, T.; et al. 2022. Bridging the gap to real-world object-centric learning. *arXiv preprint arXiv:2209.14860*.

Shen, X.; Liu, F.; Dong, H.; Lian, Q.; Chen, Z.; and Zhang, T. 2020. Disentangled generative causal representation learning.

Squires, C.; Seigal, A.; Bhate, S. S.; and Uhler, C. 2023. Linear causal disentanglement via interventions. In *International conference on machine learning*, 32540–32560. PMLR.

Wang, S.; Chen, Y.; He, Z.; Yang, X.; Wang, M.; You, Q.; and Zhang, X. 2023. Disentangled representation learning with causality for unsupervised domain adaptation. In *Proceedings of the 31st ACM international conference on multimedia*, 2918–2926.

Wang, Y.; and Jordan, M. I. 2024. Desiderata for representation learning: A causal perspective. *Journal of Machine Learning Research*, 25(275): 1–65.

Wendong, L.; Kekić, A.; von Kügelgen, J.; Buchholz, S.; Besserve, M.; Gresele, L.; and Schölkopf, B. 2023. Causal component analysis. *Advances in Neural Information Processing Systems*, 36: 32481–32520.

Xu, D.; Yao, D.; Lachapelle, S.; Taslakian, P.; Von Kügelgen, J.; Locatello, F.; and Magliacane, S. 2024. A sparsity principle for partially observable causal representation learning. *arXiv preprint arXiv:2403.08335*.

Xu, J.; De Mello, S.; Liu, S.; Byeon, W.; Breuel, T.; Kautz, J.; and Wang, X. 2022. Groupvit: Semantic segmentation emerges from text supervision. In *Proceedings of the IEEE/CVF conference on computer vision and pattern recognition*, 18134–18144.

Yang, M.; Liu, F.; Chen, Z.; Shen, X.; Hao, J.; and Wang, J. 2021. Causalvae: Disentangled representation learning via neural structural causal models. In *Proceedings of the IEEE/CVF conference on computer vision and pattern recognition*, 9593–9602.

Zitkovich, B.; Yu, T.; Xu, S.; Xu, P.; Xiao, T.; Xia, F.; Wu, J.; Wohlhart, P.; Welker, S.; Wahid, A.; et al. 2023. Rt-2: Vision-language-action models transfer web knowledge to robotic control. In *Conference on Robot Learning*, 2165–2183. PMLR.

Dataset Details

This section provides further details on the datasets used in our evaluation.

ProcTHOR The ProcTHOR dataset (Deitke et al. 2022) provides synthetic indoor scenes. For our single-object scenes, each scene contains one manipulated object, ensuring a clear focus on the intervention. In multi-object scenes, multiple objects are present, increasing the visual complexity of the scene, although only one object is again manipulated. We follow the dataset generation and filtering procedures as described in (Liu et al. 2023) to ensure consistency with the Causal Triplet benchmark.

Epic-Kitchens The Epic-Kitchens dataset (Damen et al. 2022) comprises real world egocentric videos of diverse kitchen activities. From this, we extract pre- and post-intervention image pairs. Unlike synthetic environments, Epic-Kitchens introduces significant real world challenges such as camera motion, varying lighting conditions, occlusions and dynamic backgrounds, making the task of isolating interventions particularly challenging. To ensure dataset quality, a two-stage filtering process using Grounding DINO (Liu et al. 2024) for zero-shot object detection is applied. For each extracted pair, the pipeline verifies that the target object appears clearly in both frames with a detection confidence above a set threshold $t = 0.45$. This automated filtering removes cases with poor object visibility or excessive motion blur.

Visualizations of OOD Shifts

Figures 6, 7 and 8 visually illustrate the compositional and systematic distribution shifts utilized in the Causal Triplet benchmark.

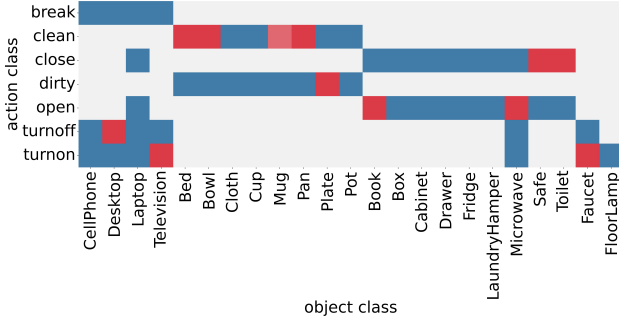


Figure 6: Compositional Distribution Shift in the ProcThor dataset. Blue boxes indicate IID data, while red boxes indicate novel OOD action-object combinations.

Geometric Analysis of Causal Delta Embeddings

This section provides additional analysis of the geometric properties of the learned Causal Delta Embeddings, complementing the insights presented along with the experimental results.

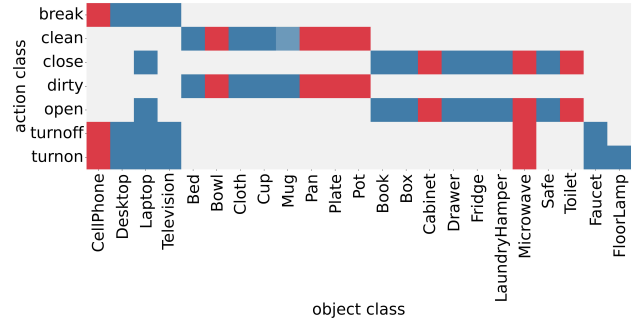


Figure 7: Systematic Distribution Shift in the ProcThor dataset. Blue boxes indicate IID data, while red boxes indicate novel OOD objects that the model has not encountered during training.

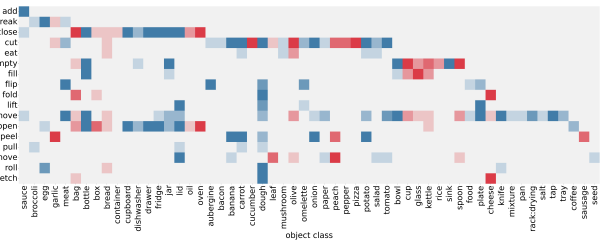


Figure 8: Systematic Distribution Shift in the EpicKitchens dataset. Blue boxes indicate IID data, while red boxes indicate novel OOD objects that the model has not encountered during training.

Analysis of Learned Action Representations To study the properties of the action representations resulting from our method, we first tested if the resulting delta embeddings could reliably predict the outcome of an intervention. To do this, for each sample in the OOD test set, we took the ‘before’ state embedding (z) and added the corresponding average action vector (μ_{action}) that was computed using the training set samples. We then measured the cosine similarity between this predicted ‘after’ state and the ground-truth ‘after’ state (\tilde{z}). Our framework showed remarkable predictive power, achieving an average cosine similarity of 0.98 in the single object systematic shift setting. This near perfect score confirms that the learned action prototypes function as true, generalizable transformation vectors, providing strong evidence that our model has learned the underlying mechanics of interventions.

UMAP Projection Figures 9 and 11 present the UMAP projection of individual delta embeddings from the IID and OOD test set of the single-object environment respectively. The delta embeddings in the IID setting achieve a clear separation between each action, leading to a near perfect IID accuracy as was presented by our experiments. On the other hand, while strong intra-class cohesion is visible, the global separation between these action clusters is not always visually distinct in the OOD setting. This suggests that while representations remain locally coherent, action representations

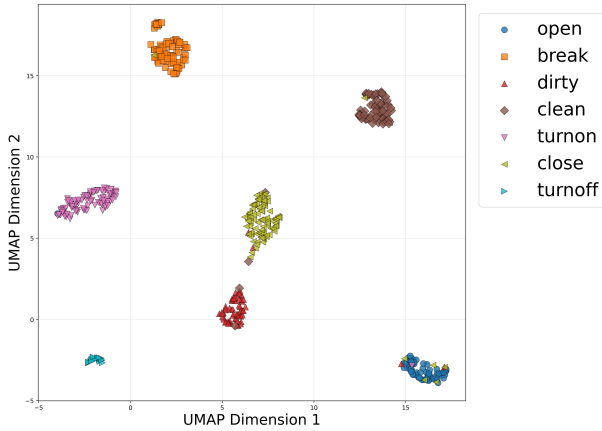


Figure 9: UMAP projection of individual delta embeddings from the IID test set. Embeddings are shaped by their ground-truth action. The plot reveals strong global separation between different action clusters.

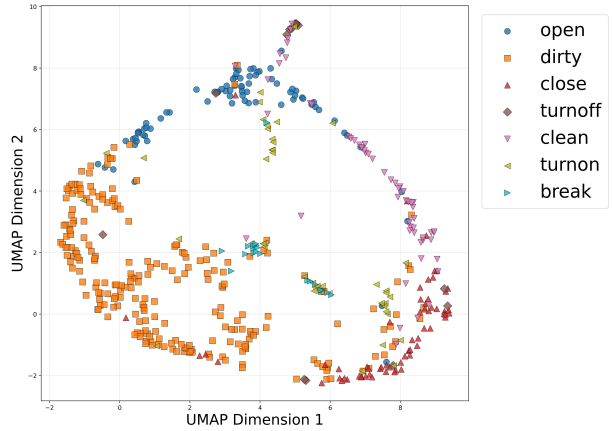


Figure 11: UMAP projection of individual delta embeddings from the OOD test set. Embeddings are shaped by their ground-truth action. The plot reveals strong local cohesion (points of the same shape cluster together) but shows a lack of clear global separation between the different action clusters.

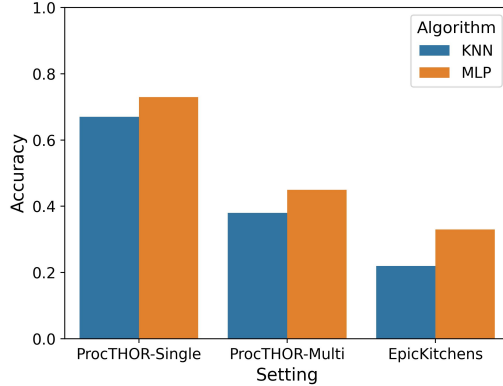


Figure 10: Comparison of classifier performance on OOD test sets. The k-NN classifier, is able to classify OOD samples if trained with Delta Embeddings.

are not as clearly discriminated compared to the IID setting. It is worth mentioning, however, that the 2D projection may not fully capture the features of the high-dimensional latent space.

k-NN Classifier Performance To quantitatively assess the quality of the local structure of the learned representations, we evaluate the performance of a simple, non-parametric k-Nearest Neighbors (k-NN) classifier directly on the Causal Delta Embeddings, where we set the number of neighbors $k = 5$. A high k-NN accuracy indicates that the local neighborhoods are semantically meaningful and highly predictive of the action class. Figure 10 compares the k-NN classifier accuracy with the use of CDE with an MLP head (as in Figure 3) across all three benchmark settings. Although k-NN does not match the effectiveness of the MLP head, it still achieves comparable results in novel OOD samples, especially in the synthetic dataset. This pro-

vides an indication that the invariance property holds in the OOD case.

Ablation Studies

In order to understand the effectiveness of each component of our method, we conducted a series of ablation studies to evaluate the impact of different backbone architectures, the impact of loss hyperparameters α and the impact of the hyperparameter k in the Top-K selection procedure for our Patch-Wise model. All the subsequent experiments ran on the single-object systematic shifts setting, except for the Top-K ablation study which ran on the multi-object systematic shifts setting.

Table 5 compares the OOD performance of the best configuration for each backbone against the benchmark’s state-of-the-art ResNet-18 result. Our final ViT-based model significantly outperforms the best ResNet-based model, demonstrating that while the richer features from ViT enhance performance, the substantial gains are primarily driven by our proposed CDE learning framework.

Table 5: Comparison of OOD performance with different backbone architectures on the single-object systematic shift benchmark.

Backbone	Method	OOD Acc. (%)
ResNet-18	(Liu et al. 2023)	0.54
ResNet-18	Ours*	0.45
ViT-Small	Ours (CE Only)	0.59
ViT-Small	Ours (Full Model)	0.73

* Best ResNet performance from our experiments was with CE + Con Loss.

Impact of Backbone Architecture

To isolate the contribution of our CDE framework from the choice of feature extractor, we conducted a controlled comparison between our ViT-Small backbone and the ResNet-18 backbone used in the original Causal Triplet benchmark.

Impact of Loss Hyperparameters

In order to select values for α_{contrast} and α_{sparsity} , we conducted an ablation study comparing various values and combinations between them. Table 6 compares some of the combinations of the values that we experimented with. Selecting a larger value for α_{contrast} , rather than α_{sparsity} , helps the model learn better representations, thus achieving better OOD accuracy. We set $\alpha_{\text{contrast}} = 2.0$ and $\alpha_{\text{sparsity}} = 1.0$ in all our main experiments.

Table 6: Comparison of various hyperparameter values for α_{contrast} and α_{sparsity} on the single-object systematic shift benchmark.

α_{contrast}	α_{sparsity}	OOD Acc. (%)
0.0	0.0	0.21 ± 0.02
0.1	1.0	0.27 ± 0.11
1.0	0.1	0.28 ± 0.04
0.5	0.5	0.29 ± 0.07
1.0	2.0	0.31 ± 0.07
2.0	1.0	0.33 ± 0.07

Top-K selection

In order to select the hyperparameter k in multi-object and real world data settings, we executed an ablation study to understand the sensitivity of our method to this parameter. As presented in Table 7, we can see that OOD accuracy increases as k increases too. This observation makes sense, since bigger objects (e.g. Fridge, Bed) would need more patches for their representations in order to be captured effectively. Thus, we set the value of $k = 4$ across all our multi-object and real world experiments.

Table 7: Comparison of OOD performance with k values for the patch selection process in multi-object settings.

k	ProcTHOR	EpicKitchens
$k = 1$	0.42 ± 0.07	0.12 ± 0.03
$k = 2$	0.45 ± 0.06	0.13 ± 0.03
$k = 3$	0.47 ± 0.04	0.13 ± 0.02
$k = 4$	0.48 ± 0.04	0.15 ± 0.02

Experimental Details

Hyperparameters

Table 8 summarizes the key hyperparameters used across all experiments. These values were selected based on ablation studies and remained consistent across different experimental settings unless otherwise noted.

Table 8: Summary of hyperparameters used across all experiments.

Parameter	Value
Learning Rate	1×10^{-4}
Backbone LR	1×10^{-5}
Batch Size	128
Epochs	50 (100 for Epic-Kitchens)
Weight Decay	0.05
α_{contrast}	2.0
α_{sparsity}	1.0
Temperature (τ)	0.07
Top-K (k)	4
Embedding Dim. (l)	256 (512 for Epic-Kitchens)
Input Resolution	224×224

Code Infrastructure

All experiments were run on a NVIDIA A100 GPU with the Slurm Workload Manager. The code was implemented in Python, using the Pytorch library. Each run takes approximately one hour to complete for the ProcTHOR and two hours for the Epic-Kitchens dataset.

Image Augmentations

We do not apply any augmentations to the images, since we do not want to modify the interventional nature of the pairs. Augmentation in this problem could harm our assumptions. For example, a rotation could affect Equation (1) and eliminate the faithfulness of the encoder. We leave it as future work to investigate whether augmentations can boost OOD performance under different assumptions. We only resize images to 224×224 pixels and apply zero-mean normalization with unit variance.

Optimization

We use a batch size of 128 and an AdamW (Loshchilov and Hutter 2017) optimizer with a cosine annealing learning scheduler for 50 epochs. In the real world setting, we instead train for 100 epochs. The ViT feature extractor is not frozen but fine-tuned with a reduced learning rate of 10% of the network’s base learning rate, which is set to 1×10^{-4} . The weight decay parameter is 0.05. All reported results include standard deviations computed over three independent runs with different random seeds.